Inorg. Chem. **2008**, *47*, 1576−1585

Tetranuclear Co^{II}, Mn^{II}, and Cu^{II} Complexes of a Novel Binucleating Pyrazolate Ligand Preorganized for the Self-Assembly of Compact [2 × 2]-Grid Structures

Jarl Ivar van der Vlugt,[†] **Serhiy Demeshko**, **Sebastian Dechert**, **and Franc Meyer***

Institut für Anorganische Chemie, Georg-August-Universität Göttingen, Tammanstrasse 4, D-37077 Göttingen, Germany

Received October 2, 2007

A straightforward synthesis toward the preparation of the rigid pyrazolate ligand $\mathbf{L}^{H}$ featuring bipyridyl side-arms is described, starting from 2,2′-bipyridyl-*N*-oxide as the sole organic building block. In this context, optimized procedures for the synthesis of the organic intermediates 6-acetyl-2,2′-bipyridine **1** and 6-methylcarboxy-2,2′-bipyridine **2** are reported. The new ligand comprises two proximate terpyridine-like binding sites and is shown to form discrete [2 × 2]-grid complexes with Co^{II}, Mn^{II}, and Cu^{II} in a highly selective self-assembly process, even in the presence of excess metal precursor. The thus obtained complexes $[Co_4L_4][Na(NO_3)_4](NO_3)$ (**3**), $[Mn_4L_4](PF_6)_4$ (**4**), and $[Cu_4L_4](ClO_4)_4$ (**5**) are fully characterized, including X-ray crystallographic analyses, and their magnetic properties are discussed. All three complexes show weak to moderate antiferromagnetic coupling between the four nuclei. The stability of the grid structures proved very high, as dissociation or exchange between metal ions in solution was not observed in a set of competition experiments.

Introduction

(Poly)pyridyl-derived ligands have found widespread use as building blocks for the formation of self-assembled supramolecular coordination complexes with an array of transition metal ions and a variety of different structures,[1,2] e.g., helical polymers,[3] linear or dendritic polymers,[4] and so-called [n × n] grid-structures.[5] Not only are these multinuclear architectures the result of elegant and highly selective self-assembly processes, but potential applications include molecular magnets, sensors, and ion-encapsulating containers.[5,6] In a common structural motif for compartmental binucleating oligopyridyl ligands (**A**), two bipyridine (bpy) subunits are linked via a central bridging unit whose

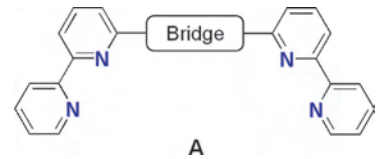

A

Figure 1. Schematic representation of compartmental oligopyridyl ligands with a (potentially coordinating) bridging unit.

flexibility and potential coordinating ability will direct the outcome of the assembly process and the overall structure(s) formed (Figure 1).

When the bridge contains additional and suitably positioned N donor atoms, two proximate metal ion binding sites related to the generic terpyridine type may result. Notable examples comprise, inter alia, rigid 2,7-naphthyridine,[7] pyrimidine (**B**),[8] imidazole (**C**),[9] or pyridazine (**D**)[10] as core fragments, in each case flanked by two bipyridyl (or phenan-

* To whom correspondence should be addressed. E-mail: franc.meyer@chemie.uni-goettingen.de.

[†] Current address: Department of Chemical Engineering and Chemistry, Eindhoven University of Technology, 5600 MB Eindhoven, The Netherlands. E-mail: j.i.v.d.vlugt@tue.nl.

(1) Fallahpour, R.-A. *Curr. Org. Synth.* **2006**, *3*, 19–39.
(2) Hofmeier, H.; Schubert, U. S. *Chem. Soc. Rev.* **2004**, *33*, 373–399.
(3) Constable, E. C.; Heirtzler, F.; Neuburger, M.; Zehnder, M. *J. Am. Chem. Soc.* **1997**, *119*, 5606–5617.
(4) Schubert, U. S.; Eschbaumer, C. *Angew. Chem., Int. Ed.* **2002**, *41*, 2892–2926.
(5) Ruben, M.; Rojo, J.; Romero-Salguero, F. J.; Uppadine, L. H.; Lehn, J.-M. *Angew. Chem., Int. Ed.* **2004**, *43*, 3644–3662.
(6) Waldmann, O. *Coord. Chem. Rev.* **2005**, *249*, 2550–2566.
(7) Plante, J. P.; Jones, P. D.; Powell, D. R.; Glass, T. E. *Chem. Commun.* **2003**, 336–337.
(8) (a) Hanan, G. S.; Volkmer, D.; Schubert, U. S.; Lehn, J. M.; Baum, G.; Fenske, D. *Angew. Chem., Int. Ed.* **1997**, *36*, 1841–1844. (b) Bassani, D. M.; Lehn, J. M.; Fromm, K.; Fenske, D. *Angew. Chem., Int. Ed.* **1998**, *37*, 2364–2367.
(9) Slater, J. W.; Steel, P. J. *Tetrahedron Lett.* **2006**, *47*, 6941–6943.
(10) (a) Brown, D.; Muranjan, S.; Jang, Y.; Thummel, R. *Org. Lett.* **2002**, *4*, 1253–1256. (b) Brown, D.; Zong, R.; Thummel, R. P. *Eur. J. Inorg. Chem.* **2004**, 3269–3272.

10.1021/ic701951a CCC: $40.75
Published on Web 02/01/2008

trolyl) units. 2,2′:6′,2″-terpyridine (tpy) usually forms complexes $[M(tpy)_2]^{x+}$ with octahedrally coordinated metal ions, where the planes of the two tpy ligands are mutually orthogonal.[11] Type **B** and **C** bis(terpyridine) chelators are thus well adapted for the self-assembly of [2 × 2]-gridlike metal ion arrays with intermetallic distances of 6.0–6.5 Å.[5] No grid-type complexes have been reported for type **D** ligands yet.

The pyrazolate heterocycle is well-known to be able to span two metal ions in a μ-η^1:η^1 fashion with metal−metal distances usually in the range of 3.2–4.5 Å.[12] Enhanced preorganization of the bimetallic array is achieved by incorporating the pyrazolate bridging unit into more elaborate compartmental binucleating ligand scaffolds.[13] The nature of the additional donor atoms appended to the 3- and 5-positions of the heterocycle and their spatial orientation toward the central pyrazolate ring can strongly govern crucial parameters such as the intramolecular metal−metal distance and the individual metal ion coordination spheres,[14] and therewith influence, e.g., the observed catalytic activity[15–17] or magnetic properties of dinuclear or polynuclear compounds.[18] Selected examples of pyrazolate-based ligands with side-arms that contain pyridyl groups are collected in Figures 2 and 3.

Ligand **E** after deprotonation provides two tripodal tetradentate metal ion binding sites, each reminiscent of the classical tris(pyridylmethyl)amine (tpa) system.[19] Bimetallic complexes of **E** (as well as various other related pyrazolate ligands) have proven quite valuable for emulating structural

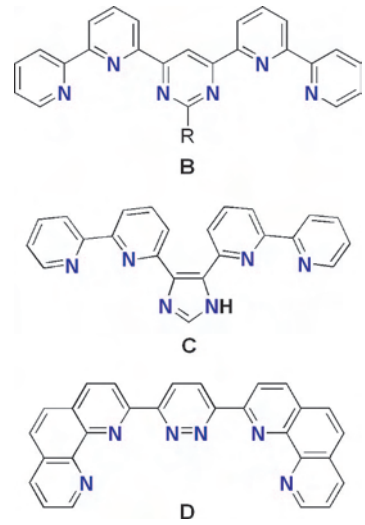

Figure 2. Representative examples of binucleating ligands containing two terpyridine-type binding compartments, all shown in their planar all-syn conformation.

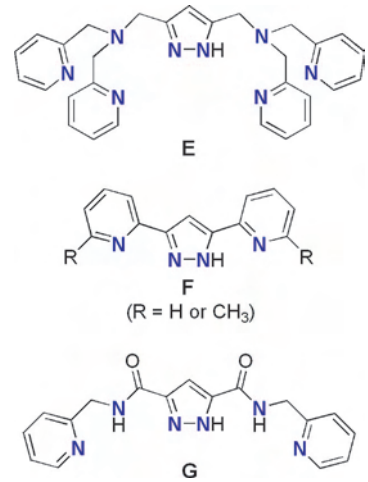

Figure 3. Representative pyrazolate-based binucleating ligands with side arms containing pyridyl groups.

and functional aspects of binuclear metallobiosites.[16,17,20] Ligands bearing simple pyridyl side arms in the 3- and 5-positions of the pyrazole (**F**) usually give bis(pyrazolato)-bridged complexes with a ligand to metal ratio 2:2.[21,22] Notable exceptions are a tetranuclear Cu^{II} complex of **F**[23] and as well as a dinuclear complex containing two Ru^{II}(tpy)

(11) Constable, E. C. *Chem. Soc. Rev.* **2007**, *36*, 246–253.
(12) La Monica, G.; Ardizzoia, G. A. *Prog. Inorg. Chem.* **1997**, *46*, 151–238.
(13) Klingele, J.; Dechert, S.; Meyer, F. *Coord. Chem. Rev.*, in preparation.
(14) (a) Meyer, F.; Beyreuther, S.; Heinze, K.; Zsolnai, L. *Chem. Ber./Recueil* **1997**, *130*, 605–613. (b) Konrad, M.; Meyer, F.; Heinze, K.; Zsolnai, L. *J. Chem. Soc., Dalton Trans.* **1998**, 199–205. (c) Meyer, F.; Heinze, K.; Nuber, B.; Zsolnai, L. *J. Chem. Soc., Dalton Trans.* **1998**, 207–213. (d) Buchler, S.; Meyer, F.; Jacobi, A.; Kircher, P.; Pritzkow, H. *Z. Naturforsch.* **1999**, *54b*, 1295–1306. (e) Prokofieva, A.; Prykhod'ko, A. I.; Dechert, S.; Enyedy, E. A.; Farkas, E.; Maringgele, W.; Demeshko, S.; Meyer, F. *Inorg. Chem.* **2007**, *46*, 4298–4307.
(15) Noël, G.; Röder, J. C.; Dechert, S.; Pritzkow, H.; Bolk, L.; Mecking, S.; Meyer, F. *Adv. Synth. Catal.* **2006**, *348*, 887–897.
(16) (a) Bauer-Siebenlist, B.; Meyer, F.; Farkas, E.; Vidovic, D.; Cuesta-Seijo, J. A.; Herbst-Irmer, R.; Pritzkow, H. *Inorg. Chem.* **2004**, *43*, 4189–4202. (b) Bauer-Siebenlist, B.; Meyer, F.; Farkas, E.; Vidovic, D.; Dechert, S. *Chem.—Eur. J.* **2005**, *11*, 4349–4360. (c) Bauer-Siebenlist, B.; Dechert, S.; Meyer, F. *Chem.—Eur. J.* **2005**, *11*, 5343–5352. (d) Meyer, F. *Eur. J. Inorg. Chem.* **2006**, 3789–3800.
(17) (a) Ackermann, J.; Meyer, F.; Kaifer, E.; Pritzkow, H. *Chem.—Eur. J.* **2002**, *8*, 247–258. (b) Ackermann, J.; Buchler, S.; Meyer, F. *C.R. Chim.* **2007**, *10*, 421–432. (c) Prokofieva, A.; Prykhod'ko, A. I.; Dechert, S.; Meyer, F. *Chem. Commun.* **2008**, DOI: 10.1039/b718162k..
(18) (a) Leibeling, G.; Demeshko, S.; Bauer-Siebenlist, B.; Meyer, F.; Pritzkow, H. *Eur. J. Inorg. Chem.* **2004**, 2413–2420. (b) Demeshko, S.; Leibeling, G.; Maringgele, W.; Meyer, F.; Mennerich, C.; Klauss, H.-H.; Pritzkow, H. *Inorg. Chem.* **2005**, *44*, 519–528. (c) Meyer, F.; Demeshko, S.; Leibeling, G.; Kaifer, E.; Pritzkow, H. *Chem.—Eur. J.* **2005**, *11*, 1518–1526. (d) Leibeling, G.; Demeshko, S.; Dechert, S.; Meyer, F. *Angew. Chem., Int. Ed.* **2005**, *44*, 7111–7114. (e) Demeshko, S.; Leibeling, G.; Dechert, S.; Meyer, F. *Dalton Trans.* **2006**, 3458–3465.
(19) Ackermann, J.; Meyer, F.; Pritzkow, H. *Inorg. Chim. Acta* **2004**, *357*, 3703–3711.
(20) (a) Meyer, F.; Pritzkow, H. *Chem. Commun.* **1998**, 1555–1556. (b) Meyer, F.; Kaifer, E.; Kircher, P.; Heinze, K.; Pritzkow, H. *Chem.—Eur. J.* **1999**, *5*, 1617–1630. (c) Meyer, F.; Hyla-Kryspin, I.; Kaifer, E.; Kircher, P. *Eur. J. Inorg. Chem.* **2000**, 771–781. (d) Buchler, S.; Meyer, F.; Kaifer, E.; Pritzkow, H. *Inorg. Chim. Acta* **2002**, *337*, 371–386. (e) Kryatov, S. V.; Rybak-Akimova, E. V.; Meyer, F.; Pritzkow, H. *Eur. J. Inorg. Chem.* **2003**, 1581–1590.
(21) Ball, P. W.; Blake, A. B. *J. Chem. Soc. A* **1969**, 1415–1422.
(22) (a) Casabó, J.; Pons, J.; Siddiqi, K. S.; Teixidor, F.; Molins, E.; Miravitlles, C. *J. Chem. Soc., Dalton Trans.* **1989**, 1401–1403. (b) Suemura, N.; Ohama, M.; Kaizaki, S. *Chem. Commun.* **2001**, 1538–1539. (c) Pons Picart, J.; Sanchez, F. J.; Casabó, J.; Rius, J.; Alvarez-Larena, A.; Ros, J. *Inorg. Chem. Commun.* **2002**, *5*, 130–133. (d) Nakano, K.; Kawata, S.; Yoneda, K.; Fuyuhiro, A.; Yagi, T.; Nasu, S.; Morimoto, S.; Kaizaki, S. *Chem. Commun.* **2004**, *289*, 2–2893. (e) Yoneda, K.; Nakano, K.; Fujioka, J.; Yamada, K.; Suzuki, T.; Fuyuhiro, A.; Kawata, S.; Kaizaki, S. *Polyhedron* **2005**, *24*, 2437–2442.
(23) Pons, J.; Sanchez, F. J.; Casabó, J.; Alvarez-Larena, A.; Piniella, J. F.; Ros, J. *Inorg. Chem. Commun.* **2003**, *6*, 833–836.

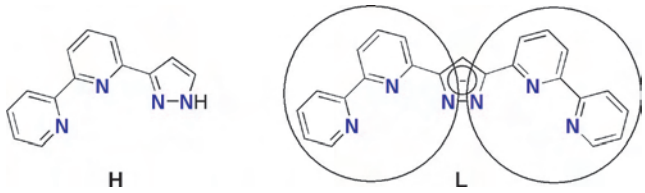

Figure 4. Terdentate pyrazole ligand **H** and target bridging ligand **L** that features two proximate terpyridine-type binding sites.

moieties, which has been shown to catalytically oxidize water in the presence of strong oxidants such as Ce^{IV}.[24] It would certainly be interesting to expand the rigidity and denticity of the side-arms of type **F** systems by introducing additional pyridine or other functional units at the R sites. The pyrazole-3,5-dicarboxamide ligand **G** in its doubly deprotonated form was recently shown to give very stable [2 × 2]-grid complexes with Cu^{II} and low-spin Ni^{II}, i.e. with metal ions that prefer square-planar or square-pyramidal coordination, but not with any metal ions that require an octahedral environment.[25] In view of the excellent bridging properties of the pyrazolate heterocycle, complexes with grid-type architectures based on other pyrazole-derived ligands are surprisingly rare.[23,26,27] [2 × 2]-grid complexes with Cu^{II} have been reported for 3-(2-pyridyl)pyrazole and its congener 6-(3-pyrazolyl)-2,2′-bipyridine (**H**; Figure 4). In the latter case, the chelate arm constitutes a single terdentate tpy-like binding site involving one of the pyrazole-N atoms, while the other pyrazole-N after deprotonation adds the bridging function toward an adjacent metal ion.

We decided to combine the favorable properties of 2,2′:6′,2″-terpyridine metal-binding domains and pyrazolate bridges in a new hexadentate, dinucleating ligand $\mathbf{L}^{H}$, to be assembled from a bipyridylketone and bipyridylester, that in its deprotonated form **L** would represent a binucleating version of **H** with two proximate tpy-like terdentate binding pockets (Figure 4). While **L** is somewhat similar to the ligand scaffolds **B**−**D** mentioned above, the pyrazolate bridging unit was expected to provide unique (and potentially beneficial) properties for the resulting oligonuclear complexes. First, due to the orientation of the N donor atoms and the close proximity of the binding compartments, the new ligand should favor relatively short metal−metal separations (compared to **B** and **C**). Second, the anionic nature of the central pyrazolate in **L** should impart particular stability to the metal complexes and reduce the overall positive charge that would be present in oligonuclear complexes with M^{II} ions (compared to ligands such as **D**). It was thus anticipated that **L** would form highly stable and extremely compact [2 × 2]-grid systems with various metal ions, in particular with metal ions that prefer octahedral coordination and as such complement the scope of geometries covered with ligand **G**. The synthesis of $\mathbf{L}^{H}$ and the isolation of its complexes with Mn^{II}, Co^{II}, and Cu^{II} are reported here. All three complexes have been characterized by UV/vis-spectroscopy, X-ray crystallography, and magnetic susceptibility measurements.

Scheme 1. General Synthesis of the Novel Ligand $\mathbf{L}^{H}$ [a]

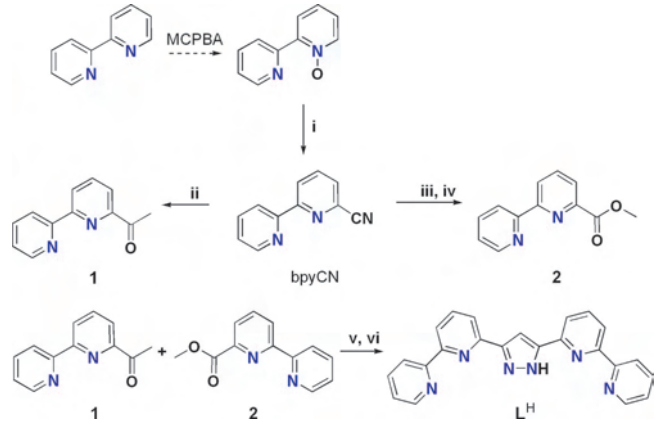

[a] (i) Me_3SiCN (4 equiv), PhCOCl (2 equiv), CH_2Cl_2, rt, 16 h, 78%; (ii) MeMgBr, Et_2O, −15 °C, 63%; (iii) NaOMe, MeOH, 16 h, rt, then AcOH; (iv) MeOH, H_2SO_4, 2 h, then NaOH, rt, 73% (steps iii and iv combined); (v) NaH, THF, 0 °C → rt, 5 h; (vi) $H_2NNH_2 \cdot H_2O$, toluene, Δ, 16 h, 39% (step v and vi combined).

Results and Discussion

Ligand Synthesis. The overall synthesis of compound $\mathbf{L}^{H}$ is a multistep process, with 2,2′-bipyridine- *N*-oxide as the sole starting material for both key intermediates **1** and **2** (Scheme 1), although **1** can also be prepared from 2-acetyl-6-bromopyridine, utilizing Rieke's zinc reagent in the three-step synthesis, but with lower overall yield.[28] Compound $\mathbf{L}^{H}$ was obtained as a white powder in 39% yield from the pseudo-Claisen condensation of 6-acetyl-2,2′-bipyridine (**1**) and 6-methylcarboxy-2,2-bipyridine (**2**), followed by a ring-closing condensation with hydrazine. $\mathbf{L}^{H}$ is soluble in organic solvents such as CH_2Cl_2, MeCN, and MeOH and has been fully characterized by NMR spectroscopy, EI mass spectrometry, and microanalysis. The UV−vis spectrum for $\mathbf{L}^{H}$ in MeOH showed three bands at λ_{max} (ε [L mol^{-1} cm^{-1}]) 237 (32 550), 263 (30 230), and 306 nm (23 760), attributed to various $\pi^* \leftarrow \pi$ transitions (Figure S1 in the Supporting Information).

Synthesis, Spectroscopic Characterization, and Molecular Structures of Metal Complexes. Deprotonation of $\mathbf{L}^{H}$ with 1 equiv NaO^{t}Bu and subsequent addition of 1 equiv $Co(NO_3)_2 \cdot 6H_2O$ in MeOH yielded a deep-yellow solution, and removal of the solvent left a yellow solid. The UV–vis spectrum for **3** in MeOH (Figure S2 in the Supporting Information) showed intense $\pi^* \leftarrow \pi$ bands, which were shifted with respect to the free ligand, plus a shoulder band at 454 nm (ε 5520 L mol^{-1} cm^{-1}), possibly indicative of

(24) (a) Catalano, V. J.; Craig, T. J. *Inorg. Chem.* **2003**, *42*, 321–334. (b) Sens, C.; Romero, I.; Rodriguez, M.; Llobet, A.; Parella, T.; Benet-Buchholz, J. *J. Am. Chem. Soc.* **2004**, *126*, 7798–7799.
(25) Klingele, J.; Prykhod'ko, A. I.; Demeshko, S.; Dechert, S.; Meyer, F. *Dalton Trans.* **2007**, 2003–2013.
(26) Zhang, H.; Fu, D.; Ji, F.; Wang, G.; Yu, K.; Yao, T. *J. Chem. Soc., Dalton Trans.* **1996**, 3799.
(27) Mann, K. L. V.; Psillakis, E.; Jeffery, J. C.; Rees, L. H.; Harden, N. M.; McCleverty, J. A.; Ward, M. D.; Gatteschi, D.; Totti, F.; Mabbs, F. E.; McInnes, E. J. L.; Riedi, P. C.; Smith, G. M. *J. Chem. Soc., Dalton Trans.* **1999**, 339–348.

(28) Starting from 2-acetyl-6-bromopyridine, initial protection of the keto-functionality with 1,2-ethyleneglycol, followed by Pd-catalyzed coupling with 2-pyridyl zinc bromide (Rieke's metal) in THF and subsequent acidic deprotection of the ketone group yielded **1** in an overall yield of ∼15%. Fang, Y. Q.; Hanan, G. S. *Synlett.* **2003**, 852–854.

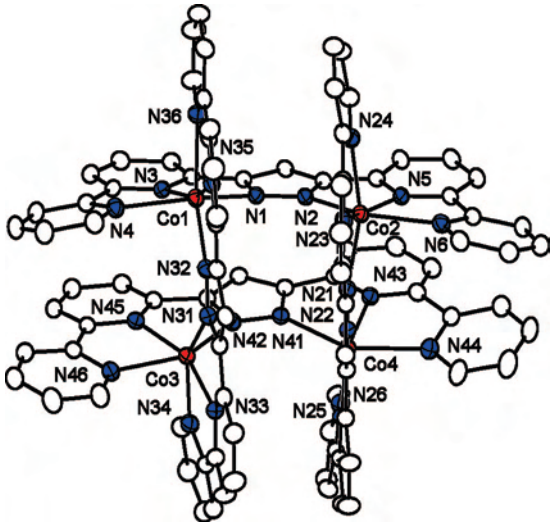

Figure 5. ORTEP plot (30% probability thermal ellipsoids) of the cationic part of complex **3**, $[Co_4\mathbf{L}_4][Na(NO_3)_4](NO_3)$. Solvent molecules, counterions, and hydrogen atoms are omitted for clarity. Selected atom distances (Å): Co1···Co2 4.4935(5), Co1···Co3 4.5056(6), Co1···Co4 6.2847(6), Co1-N1 2.101(2), Co1−N3 2.072(2), Co1−N4 2.234(2), Co1−N32 2.122(3), Co1−N35 2.078(2), Co1−N36 2.287(3), N1−N2 1.343(3). Selected bond angles (deg): N1−Co1−N3 77.51(9), N1−Co1−N4 150.11(9), N1−Co1−N32 99.48(9), N1−Co1−N35 115.81(9), N1−Co1−N36 90.39(9), N3−Co1−N4 73.85(9), N3−Co1−N32 120.31(9), N3−Co1−N35 157.37(10), N32−Co1−N35 77.22(9).

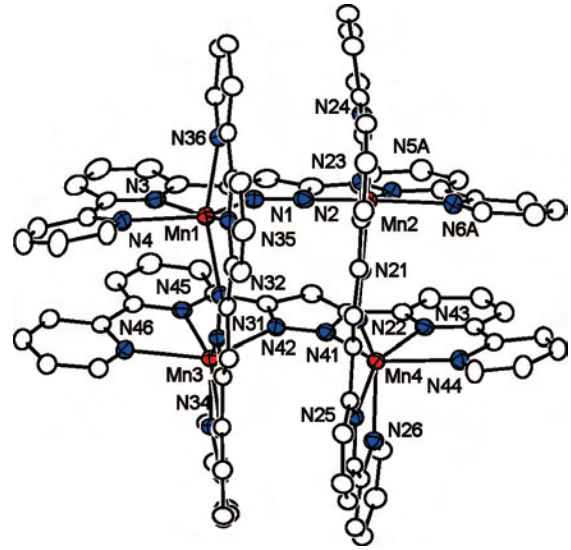

Figure 6. ORTEP plot (30% probability thermal ellipsoids) for the cation of complex **4**, $[Mn_4(\mathbf{L})_4](PF_6)_4$. Disorder and hydrogen atoms are omitted for clarity. Selected atom distances (Å): Mn1···Mn2 4.424(1), Mn1···Mn3 4.500(1), Mn1···Mn4 6.230(1), Mn1−N1 2.181(4), Mn1−N3 2.247(4), Mn1−N4 2.358(4), Mn1−N32 2.195(4), Mn1−N35 2.223(4), Mn1−N36 2.310(4), N1−N2 1.355(6). Selected bond angles (deg): N1−Mn1−N3 73.08(16), N1−Mn1−N4 142.84(16), N1−Mn1−N32 104.14(15), N1−Mn1−N35 126.92(15), N1−Mn1−N36 90.26(15), N3−Mn1−N4 69.80(17), N3−Mn1−N32 116.35(15), N3−Mn1−N35 156.65(15), N32−Mn1−N35 73.62(15).

charge-transfer involving the Co^{II} ions and weak d−d bands at 519 and 550 nm. Identical spectroscopic data were obtained with $CoCl_2{\cdot}6H_2O$ as the reagent. The solid-state (diffuse reflectance) UV−vis spectrum of **3** showed similar features, confirming that the structural motif found in the solid state is preserved in solution. Slow diffusion of Et_2O into a MeOH solution of **3** resulted in orange-red single crystals. A crystallographic analysis afforded the molecular structure as depicted in Figure 5.

As anticipated, **3** features a so-called [2 × 2]-grid structure composed of four ligands and four metal ions. It is the first such grid structure for Co to be reported with pyrazolate as the central connecting theme. Even in the presence of excess Co^{II} ions, **3** appears to be the only species formed in solution, suggesting that the ligand $\mathbf{L}^H$ strongly favors self-assembly of the [2 × 2]-grid motif. The geometry around the Co^{II} ions is distorted octahedral, evidenced by the angles N1−Co1−N4 (150.11(9)°) and N3−Co1−N4 (73.85(9)°). The distortion mainly originates from the extremely rigid binding pockets present within each ligand, with two coplanar five-membered chelate rings formed upon complexation, including one to the smaller-sized pyrazolate heterocycle, and the resulting proximity of the parallel ligand strands in the very compact grid array. Distances between some of the aromatic rings are around 3.8 Å, indicative of $\pi-\pi$ stacking. The aromatic rings alongside one ligand "plane" show some deviation from coplanarity, with dihedral angles between two pyridine rings of 6.7−17.7°.

Upon reaction of equimolar amounts of $Mn(OAc)_2$ and **L** (after deprotonation of $\mathbf{L}^H$ with NaO^{t}Bu) in a mixture of MeCN/MeOH (∼10:1),[29] followed by addition of 1 equiv of NH_4PF_6, to establish anion-exchange and facilitate formation of an isolable, discrete multinuclear species, at room temperature and stirring for 16 h, a yellow solution was obtained, which yielded a yellow solid after filtration and evaporation of the solvent. The UV−vis spectrum of **4** in MeCN (Figure S3 in the Supporting Information) showed two very faint shoulder bands at 447 and 421 nm and strong ligand-based $\pi^* \leftarrow \pi$ transitions at λ_{max} (ε [L mol^{-1} cm^{-1}]) 240 (32 550), 286 (30 230) and 341 nm (23 760).

Slow diffusion of a MeCN solution of **4** with Et_2O in air yielded bright-yellow crystals that were suitable for X-ray crystallographic analysis; Figure 6 shows the obtained molecular structure. It reveals a [2 × 2]-grid structure with Mn^{II} centers, similar to that observed with Co. It should be noted that examples of tetranuclear Mn^{II} grid structures are scarce, in particular those featuring true octahedral coordination for the Mn centers without participation of ligating solvent molecules.[30]

The geometry around the Mn ions is strongly distorted from octahedral, much as in the case of complex **3**, evidenced by the angles N1−Mn1−N4 (142.84(16)°) and N3−Mn1−N4 (69.80(17)°), which are slightly smaller compared to the analogous angles in complex **3**. Complex **4** has no mirror symmetry, as the four Mn-ions are not located at the corners of a perfect square and the coordinated ligands are not

(29) MeOH was added to improve the solubility of $Mn(OAc)_2$ in the reaction mixture. Without MeOH, the reaction suspension remained unchanged for at least 4 h.

(30) (a) Thompson, L. K.; Waldmann, O.; Xu, Z. *Coord. Chem. Rev.* **2005**, *249*, 2677–2690. (b) Ruben, M.; Lehn, J.-M.; Vaughan, G. *Chem. Commun.* **2003**, 1338–1339.

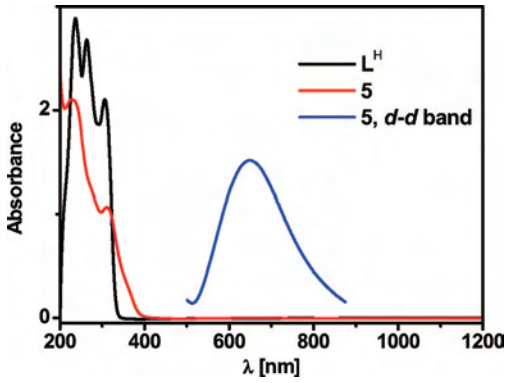

Figure 7. UV−vis spectrum of complex **5** in MeCN, compared to that of $\mathbf{L}^{H}$ in MeOH. The inset shows an enlargement of the d−d transition band observed for the Cu^{II} ions with λ_{max} 647 nm.

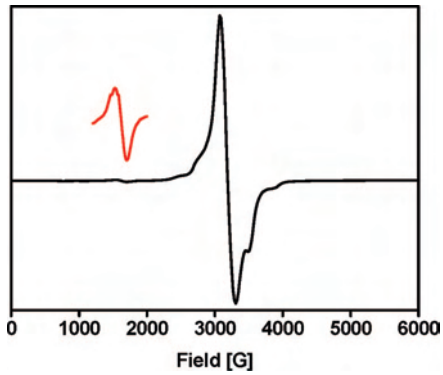

Figure 8. X-band EPR spectrum of solid **5** (black line) at $T = 135$ K. The inset (red line) shows enlargement of the "half-field" signal.

stacked properly, with dihedral angles Mn−N^{pz}−N^{pz}−Mn of the pyrazolate-bridged fragments in the range 13.6−19.6°.

Reaction of an equimolar ratio of $Cu(ClO_4)_2{\cdot}6H_2O$ and **L** (obtained by deprotation of $\mathbf{L}^{H}$ with NaO^{t}Bu) in MeCN at room temperature instantaneously produced a green solution that after 3 h of stirring and removal of the solvent resulted in a green powder. The UV−vis spectrum of complex **5** in MeCN (Figure 7) showed the typical signature for Cu^{II} ions in square-pyramidal coordination environment, with a d−d absorption maximum at 647 nm (ε = 425 L mol^{-1} cm^{-1}), as well as intense ligand-based $\pi^* \leftarrow \pi$ transitions at higher energy.

The same UV−vis spectral features were observed when **5** was measured as a solid in diffuse reflectance mode, indicative that the solid-state and solution structures involve similar coordination spheres for the Cu^{II} ions. The X-band electron paramagnetic resonance (EPR) spectrum of a solid sample of **5** at 135 K revealed a strong broad signal at 3190 G, as well as a very weak "half-field" signal at 1625 G, characteristic for an exchange-coupled system (Figure 8). No hyperfine structure due to the pyrazolate and pyridine N-donor atoms is discernible. Similar spectral features were observed in a frozen diluted solution of **5** in MeOH at 170 K, and no typical signals for any mononuclear Cu^{II} species were observed, suggesting that the tetranuclear structure exhibits high stability without any significant dissociation in solution.

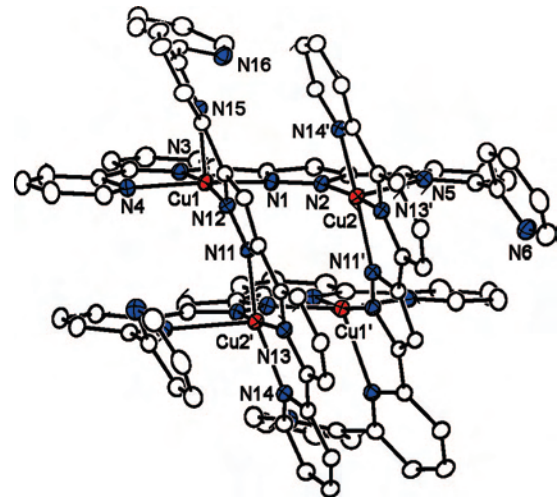

Figure 9. ORTEP plot (30% probability thermal ellipsoids) for the cation of complex **5**, $[Cu_4(\mathbf{L})_4](ClO_4)_4$. Hydrogen atoms are omitted for clarity. Selected atom distances (Å): Cu1···Cu2 4.0838(4), Cu1···Cu1′ 5.2315(5), Cu1···Cu2′ 4.1394(4), Cu2···Cu2′ 4.2308(6), Cu1−N1 1.9983(18), Cu1−N3 1.9508(19), Cu1−N4 2.0659(19), Cu1−N12 1.9597(18), Cu1−N15 2.3520(18), N1−N2 1.344(3). Selected bond angles (deg): N1−Cu1−N3 79.79(8), N1−Cu1−N4 157.90(8), N1−Cu1−N12 101.91(7), N1−Cu1−N15 109.55(7), N3−Cu1−N4 79.10(8), N3−Cu1−N12 170.06(8). Symmetry transformation used to generate equivalent atoms (′): 1 − x, y, 1.5 − z.

Slow diffusion of Et_2O into a solution of **5** in MeCN yielded green crystals suitable for X-ray crystallographic analysis. The obtained molecular structure is depicted in Figure 9.

All four Cu^{II} ions in **5** are found in a slightly distorted square-pyramidal geometry, with a τ-value[31] of 0.20 and 0.25 for Cu1 and Cu2, respectively. Five-coordination of the metal ions requires that one pyridyl unit remains uncoordinated at each corner of the [2 × 2]-grid, which is clearly different from the situation observed for complexes **3** and **4**. The inner pyridine unit from the same partly uncoordinated bipyridine sidearm represents the axial ligand on each Cu^{II} ion that displays typical Jahn–Teller elongation with bond lengths Cu−N_{eq} of 1.95−2.06 Å and Cu−N_{ax} of 2.35 Å. Although six-coordinate Cu^{II} with $\{N_6\}$ ligation from two tpy-type binding domains is well-known (usually with local D_{2d} symmetry in which the d_{x2-y2} and d_{z2} orbitals are not degenerate),[32] the distinct features of complex **5** signify a certain preference for five-coordination. The overall paddle-wheel structure of **5** with idealized C_2-symmetry, with dangling pyridine units on each face of the cubical grid structure, is reminiscent of the [2 × 2]-grid structures obtained with the diamido-pyrazolate ligand **H** reported recently.[25]

A side-view of the central cores of all three complexes, showing only the metal ions with their surrounding N-donor atoms, is presented in Figure 10. This representation reflects the roughly square arrangement of the metal ions in the Co^{II} complex **3** (left), while a more pronounced twist in the grid structure is apparent for complex **4**. In contrast to the near

(31) For the original definition of τ, see Addison, A. W.; Rao, T. N.; Reedijk, J.; van Rijn, J.; Verschoor, G. C. *J. Chem. Soc., Dalton Trans.* **1984**, 1349–1356.

(32) Chaurin, V.; Constable, E. C.; Housecroft, C. E. *New J. Chem.* **2006**, *30*, 1740–1744.

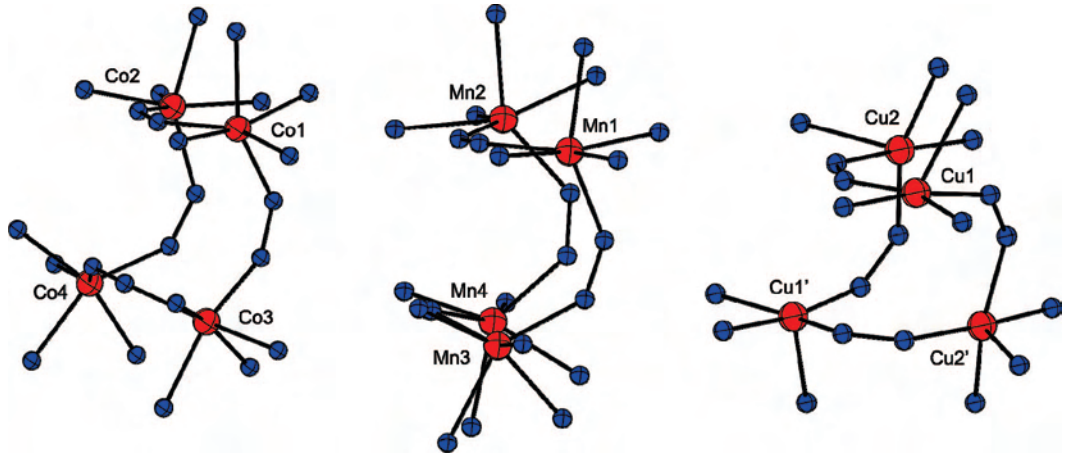

Figure 10. Side-view projections of of **3** (left), **4** (middle), and **5** (right), depicting the respective spatial arrangements of the tetranuclear metal cores of each complex.

octahedral metal ion environments in **3** and **4**, the Cu^{II} ions in **5** feature square-pyramidal coordination, which leads to a drastic twisting of the grid core with near tetrahedral spatial arrangement of the four metal centers (Figure 10, right).

Magnetic Properties of the Grid Complexes. Magnetic susceptibilities for powdered samples of single-crystalline material of complexes **3**–**5** were measured at two different magnetic fields (2000 and 5000 G) in a temperature range of 2−295 K. No significant field dependence was observed for either complex. Figure 11 shows the magnetic susceptibility χ and of the product χT vs temperature.

The observed $\chi_M T$ value at 295 K is 10.73 cm^3 K mol^{-1} (9.27 μ_B) for **3**, 17.16 cm^3 K mol^{-1} (11.72 μ_B) for **4**, and 1.65 cm^3 K mol^{-1} (3.64 μ_B) for **5**, which closely matches the value expected for four uncoupled M^{II} ions (hs-Co^{II} 9.45 μ_B for $g = 2.44$; hs-Mn^{II} 11.83 μ_B for $g = 2.00$; Cu^{II} 3.69 μ_B for $g = 2.13$). In all cases $\chi_M T$ tends toward zero at low temperature and the χ_M curve passes through a maximum, which provides evidence that all complexes have an $S = 0$ ground-state due to overall antiferromagnetic coupling between the metal ions. The position of the maxima in the χ_M curves (14 K for Co^{II}, below 5 K for Mn^{II}, 42 K for Cu^{II}), however, suggest pronounced differences in the coupling strength. Experimental data were simulated using a fitting procedure to the appropriate Heisenberg–Dirac-van-Vleck (HDvV) spin Hamiltonian for isotropic exchange coupling and Zeeman splitting (eq 1), assuming equal J values for all four metal−metal bridges.[33,34]

$$\hat{H} = -2J\Sigma\hat{S}_i\hat{S}_j + g\mu_B B\Sigma\hat{S}_{iz} \qquad (1)$$

A Curie–Weiss-behaved paramagnetic impurity (ρ) that presumably causes the increase of χ_M at very low temperatures and temperature-independent paramagnetism (TIP) were included according to $\chi = (1 - \rho)\chi + \rho\chi_{mono} + TIP$. Table 1 summarizes the magnetic parameters obtained from best fit analyses. In the Co^{II} case, including single-ion zero-field splitting parameters D and E/D in the fitting procedure did not have any major effect on the magnitude of the J value.

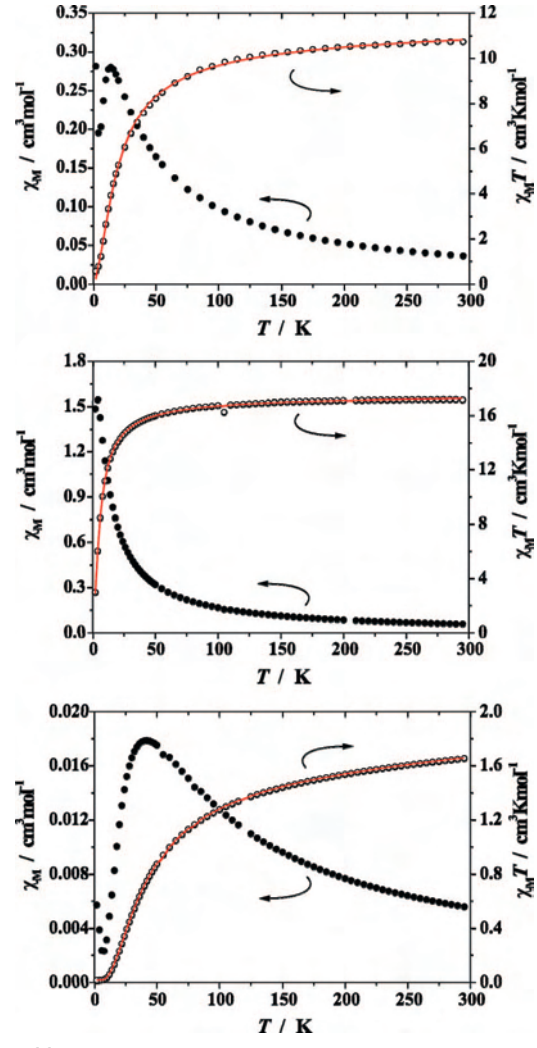

Figure 11. Plots of χ_M (solid circles) and $\chi_M T$ (open circles) versus temperature for **3** (top), **4** (middle), and **5** (bottom) at 5000 G. The red solid lines represent the calculated curve fits (see text).

For Co^{II}, the g value significantly exceeds that of the spin-only case due to non-negligible contributions of the orbital-moment component,[35] with the value of $g = 2.44$ lying well

(33) Kahn, O. *Molecular Magnetism*; Wiley-VCH, Publishers Inc.: New York, 1993.
(34) Simulation of the experimental magnetic data with a full-matrix diagonalization of exchange coupling and Zeeman splitting was performed with the julX program (Bill, E. Max-Planck Institute for Bioinorganic Chemistry: Mülheim/Ruhr, Germany).

Table 1. Best Fit Parameters of Magnetic Data Analyses for Complexes **3**−**5**

complex	g	J [cm^{-1}]	ρ [%]	TIP [cm^3 mol^{-1}]
3 (Co^{II})	2.44	−2.0	0.6	8.0E−4 (fixed)
4 (Mn^{II})	2.00	−0.25	0.6	4.0E-4 (fixed)
5 (Cu^{II})	2.13	−18.7	3.5	4.8E-4

within the range found for other N-donor-based [2 × 2]-grid structures of cobalt.[30] In agreement with the qualitative evaluation of the χ curves, the antiferromagnetic coupling is strongest (although still moderate) in the Cu^{II} case, but very weak for Mn^{II}. The result for **5** is in good agreement with reported J values for other Cu^{II} complexes which have similar symmetry properties, i.e. diazole bridges linking the four metal ions in a tetranuclear core of approximate S_4 symmetry.[25−27,36] Antiferromagnetic coupling mediated by pyrazolate bridges is well understood, and magnetostructural correlations have been established for doubly pyrazolato-bridged dicopper(II) complexes. Distortion of the Cu^{II} coordination sphere from square-pyramidal toward trigonal-bipyramidal geometry,[37] the deviation from coplanarity of the pyrazolate planes and of the copper coordination planes,[38,39] the Cu−N−N angle, and the bending angles $\delta_{pz\text{-}bend}$ (representing the dihedral angle of the pyrazolate plane relative to the Cu−N−N−Cu plane)[37,40] have been identified as crucial factors that determine the strength of the antiferromagnetic coupling. Inter alia, it has been proposed that overlap between the Cu(d_{x2-y2}) and the pyrazolate-Nσ orbitals is most effective when the angle Cu−N−N approaches 130.5°, with a quasi linear dependence of the coupling constant J on the mean deviation from this optimal value .[41] Angles Cu−N−N for **5** are found in the range 130.0–137.7°. Despite this, in the present case **5**, one might have expected an even smaller antiferromagnetic coupling than observed experimentally, since the magnetic Cu(d_{x2-y2}) orbitals of adjacent Cu^{II} ions are not far from a spatially orthogonal orientation. As mentioned above, however, many geometric parameters may contribute to the modulation of the coupling strength, which hampers any definite magnetostructural correlations for the limited number of known systems of this type.

Stability of the [2 × 2]-Grid Systems in Solution. High-resolution (HR) ESI-MS spectra of MeCN solutions of all complexes show a prominent peak characteristic for the quadruply charged ions $[M_4L_4]^{4+}$, suggesting that the grid-type arrays stay intact in solution. The spectrum for complex **4** is shown in Figure 12 as an example; spectra for **3** and **5** can be found in the Supporting Information (Figures S5 and S6).

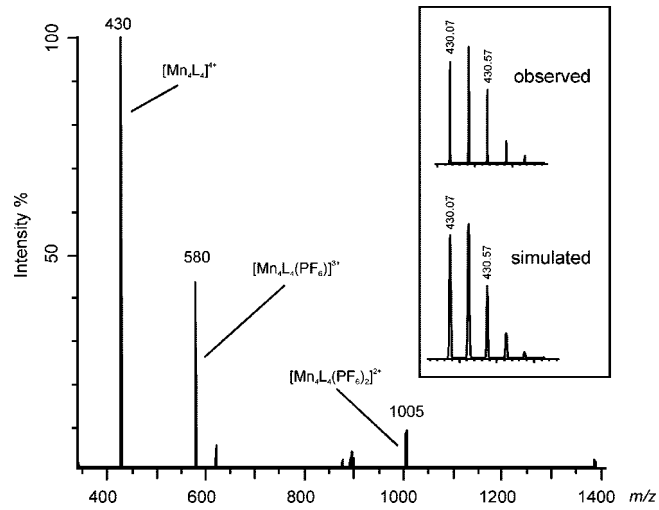

Figure 12. HRESI-MS spectrum of **4** (MeCN solution). The inset shows the observed and calculated isotopic distribution pattern for the ion $[Mn_4L_4]^{4+}$

In the case of **5**, additional peaks are observed for ions $[Cu_2L_2]^{2+}$and $[Cu_2L_2(ClO_4)]^{2+}$, which may be taken as indication that the presence of uncoordinated pyridine groups imparts a lower stability to the Cu^{II} system compared to the closed structures of **3** and **4**. However, dissolving equimolar amounts of crystalline **3** and **5** together in MeCN[42] and stirring for 16 h at room temperature did not lead to any detectable exchange of metal ions, as monitored by ESI-MS, and in fact, both green and red crystals of the individual complexes could be again obtained from the mixture in MeCN/Et_2O. Likewise, addition of $Co(NO_3)_2{\cdot}3H_2O$ to a solution of **5** in MeCN did not lead to any exchange of Cu for Co, as indicated by the absence of bands in the UV−vis spectrum corresponding to any Co^{II} complex other than the nitrate salt. This argues against any appreciable fragmentation of intact [2 × 2]-grid structures in solution also for the Cu system and testifies to the high stability of the present series of tetranuclear complexes.

Concluding Discussion. The multistep synthesis of a new polypyridyl ligand with a pyrazolate core, derived from 2,2-bipyridyl-*N*-oxide as the sole starting material, has been described. Deprotonation of $\mathbf{L}^H$ provides a monoanionic binucleating ligand with two tridentate coordinating motifs in rigid, confined binding pockets, each subunit reminiscent of the classic terpyridine ligand, but with one pyridine moiety replaced by the shared pyrazolate ring (**I** versus **J**, Figure 13).

In the absence of strongly coordinating coligands, **L** shows a high tendency toward the selective formation of stable [2 × 2]-grid structures with metal ions such as Co^{II}, Mn^{II}, and Cu^{II}, even if the stereoelectronic requirements do not favor an octahedral coordination sphere (Cu^{II}). The molecular structures of the cations $[Co_4L_4]^{4+}$ (**3**), $[Mn_4L_4]^{4+}$ (**4**), and

(35) Griffith, J. S. *Trans. Faraday Soc.* **1958**, *54*, 1109–1116.
(36) Bencini, A.; Gatteschi, D.; Zanchini, C.; Haasnoot, J. G.; Prins, R.; Reedijk, J. *J. Am. Chem. Soc.* **1987**, *109*, 2926–2931.
(37) Matsushima, H.; Hamada, H.; Watanabe, K.; Koikawa, M.; Tokii, T. *J. Chem. Soc., Dalton Trans.* **1999**, 971.
(38) Ajo, D.; Bencini, A.; Mani, F. *Inorg. Chem.* **1988**, *27*, 2437–2444.
(39) Teichgräber, J.; Leibeling, G.; Dechert, S.; Meyer, F. *Z. Anorg. Allg. Chem.* **2005**, *631*, 2613–2618.
(40) Tanase, S.; Koval, I. A.; Bouwman, E.; de Gelder, R.; Reedijk, J. *Inorg. Chem.* **2005**, *44*, 7860–7865.
(41) Hanot, V. P.; Robert, T. D.; Kolnaar, J.; Haasnoot, J. G.; Reedijk, J.; Kooijman, H.; Spek, A. L. *J. Chem. Soc., Dalton Trans.* **1996**, 4275–4281.

(42) Complex **5** did not show any appreciable solubility in MeOH, implying that degradation of this [2 × 2]-grid structure into a {MeO···HOMe}-bridged dinuclear copper(II) species (similar to complexes described in ref 14e and 17) is unlikely. Such species however can be formed with, inter alia, $Cu(NO_3)_2{\cdot}6H_2O$ as precursor and using a 2:1 Cu:$\mathbf{L}^H$ stoichiometry: van der Vlugt, J. I.; Dechert, S.; Meyer, F. unpublished results.

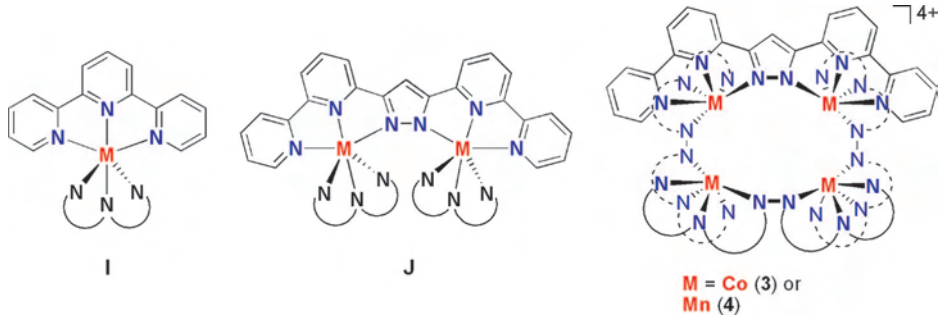

Figure 13. Analogy between the mononuclear tpy-complexes (**I**) with the binuclear version derived from deprotonated ligand $\mathbf{L}^{H}$ (**J**) and grid-type complexes reported in this work.

$[Cu_4L_4]^{4+}$ (**5**) reveal distinctly different geometries around the metal centers, with distorted octahedral arrangements for Co^{II} and Mn^{II} and square-pyramidal coordination for Cu^{II}, which results in dangling pyridyl groups and a paddlewheel-type structure in the latter case. No dissociation or scrambling of the [2 × 2]-grid cores is observed in solution. Magnetic susceptibility measurements show very weak antiferromagnetic coupling for the Co and Mn complexes and slightly higher interactions with Cu as the spin carrier.

Ligand **L** represents a binucleating scaffold with very pronounced preorganization of the two proximate binding sites, and it appears predestined for the self-assembly of [2 × 2]-grid structures with suitable metal ions. In this light, preliminary experiments indicate similar behavior toward Ni^{II} and Zn^{II}. Studies toward the preparation of Mn^{III} and Fe^{II} containing complexes with **L** are ongoing, with the aim of assembling grid-type coordination compounds with potentially interesting magnetic properties. Furthermore, the recent report of catalytic water oxidation by a pyrazolate-bridged diruthenium complex (with type **F** ligand; Figure 3)[24b] in combination with the prominence of tpy-based systems in that field suggests to use **L** as a new scaffold for functional modeling of the oxygen-evolving complex of photosystem II.

Experimental Section

General. Solvents were purified by established procedures. Starting materials were purchased from commercial sources and used as received. Microanalyses were performed by the Analytical Laboratory of the Institute for Inorganic Chemistry at Georg-August-University Göttingen. IR spectra (as KBr pellets) were recorded with a Digilab Excalibur, and UV–vis spectra of solutions and solids (diffuse reflectance) with a Varian Cary 5000 spectrometer at room temperature. Mass spectra were measured using a Finnigan MAT 8200 (EI), a Finnigan MAT 95 (FAB-MS), or a Finnigan MAT LCQ mass spectrometer (ESI-MS). NMR spectra were recorded with a Bruker Avance 200 at room temperature (^{1}H 200.13 MHz, ^{13}C 50.3 MHz) and calibrated to the residual proton and carbon signals of the solvent ($CDCl_3$ δ_H 7.26, δ_C 77.0). EPR spectra were recorded on a Bruker ELEXSYS 500 spectrometer. Magnetic data were measured with a Quantum-Design MPMS-5S SQUID magnetometer equipped with a 5 T magnet in a range from 2 to 300 K. Samples were powdered, then contained in a gel bucket, and fixed in a nonmagnetic sample holder. Each raw data file for the measured magnetic moment was corrected for the diamagnetic contribution from the sample holder and the gel bucket. The molar susceptibility was corrected for diamagnetic contributions using Pascal's constants and the increment method.

Caution! *Although no problems were encountered in this work, transition metal perchlorate complexes are potentially explosive and should be handled with care and proper precautions.*

Synthesis of 6-Cyano-2,2′-bipyridine (bpyCN) (Modification of a Literature Procedure[43]). To an ice-cooled solution of 2,2′-bipyridyl-*N*-oxide (15.26 g, 88.6 mmol) and trimethylsilyl cyanide (50 mL, 375 mmol) in ca. 250 mL dry CH_2Cl_2 under N_2 was carefully added benzoyl chloride (2 equiv, 20.4 mL, 177.2 mmol). After stirring overnight at rt, 10% aq Na_2CO_3 (200 mL) was carefully added to the chilled reaction mixture (effervescence of the solution occurs). The organic solvent was evaporated to precipitate a light-brown crude product. After removal of the water phase by filtration, the solid residue was redissolved in 100 mL CH_2Cl_2, whereafter the organic phase was washed with water, separated, dried over $MgSO_4$, and subsequently concentrated in vacuo to leave a light-yellow solid. Removal of an unidentified byproduct (signals at 7.4 and 8.1 ppm in the ^{1}H NMR spectrum, both multiplets) was achieved by washing with hexanes (2 × 50 mL). Subsequent drying in vacuo of the solid residue yielded **A** as an off-white powder (12.45 g, 68.7 mmol, 77.5%). MS (EI): *m/z* (%) = 181 (100) $[M]^+$, 155 (12) $[M\text{-}CN]^+$. ^{1}H NMR (500 MHz, $CDCl_3$): δ 7.35 (ddd, J_1 = 7.5 Hz, J_2 = 4.8 Hz, J_3 = 1.2 Hz, 1H), 7.67 (dd, J_1 = 7.6 Hz, J_2 = 1 Hz, 1H), 7.83 (td, J_1 = 7.9 Hz, J_2 = 1.8 Hz, 1H), 7.92 (t, J = 7.6 Hz, 1H), 8.44 (dt, J_1 = 7.9 Hz, J_2 = 1 Hz, 1H), 8.65 (dd, J_1 = 8.1 Hz, J_2 = 1 Hz, 1H), 8.68 (m, 1H). ^{13}C NMR ($CDCl_3$): δ 117.3, 121.6, 124.2, 124.7, 128.1, 133.2, 137.2, 137.9, 149.2, 153.9, 157.6.

Synthesis of 2-Acetyl-6(2-pyridyl)pyridine (1) (Based on a Literature Procedure[44]). To a solution of **bpyCN** (8.66 g, 47.8 mmol) in dry THF (250 mL) was added dropwise MeMgBr (3.0 M in Et_2O, 19.1 mL, 1.2 equiv, 57.4 mmol) at −15 °C. The reaction mixture was further stirred for 1 h at −15 °C and then for 2 h at rt to give an orange−red solution. Slow addition of a saturated NH_4Cl solution (200 mL) was followed by phase separation. The aqueous phase was extracted with THF (200 mL) and then CH_2Cl_2 (200 mL). The combined organic phases were washed with saturated NaCl (200 mL) and H_2O (200 mL) and then dried over $MgSO_4$. Evaporation of the filtrate in vacuo left a reddish oil. Extraction with hexane (3 × 150 mL) and removal of the solvent in vacuo yielded **1** as an off-white solid (5.91 g, 29.8 mmol, 62.5%). ^{1}H NMR (500 MHz, $CDCl_3$): δ 3.81 (s, COC H_3, 3H), 7.33 (ddd, J_1 = 7.5 Hz, J_2 = 4.6 Hz, J_3 = 1.2 Hz, 1H), 7.84 (dt, J_1 = 7.6 Hz, J_2 = 1.8 Hz, 1H), 7.93 (t, J = 7.8 Hz, 1H), 8.03 (dd, J_1 = 7.7 Hz,

(43) Heirtzler, F. R. *Synlett.* **1999**, 1203–1206.
(44) Zong, R.; Thummel, R. P. *Inorg. Chem.* **2005**, *44*, 5984–5986.

J_2 = 1.2 Hz, 1H), 8.51 (dt, J_1 = 8.0 Hz, J_2 = 1.1 Hz, 1H), 8.61 (dd, J_1 = 7.8 Hz, J_2 = 1.2 Hz, 1H), 8.68 (ddd, J_1 = 4.8 Hz, J_2 = 1.7 Hz, J_3 = 0.9 Hz, 1H). ^{13}C NMR ($CDCl_3$): δ 25.7, 121.1, 121.4, 124.1, 124.2, 137.0, 137.8, 149.2, 152.9, 155.3, 200.2.

Synthesis of 6(2,2′-Bipyridyl)methylcarboxylate (2) (Adaptation of a Literature Procedure[43]**).** A red solution of **bpyCN** (12.2 g, 67.3 mmol) and sodium methoxide (6.06 g, 112.1 mmol) in dry MeOH (200 mL) was stirred overnight under N_2 at rt. Then, AcOH (18 mL) and solid $NaHCO_3$ (15 g) were added, the mixture was stirred for 15 min and filtered to remove salts, and subsequently, the solvent was removed in vacuo. The residue was dissolved in EtOAc/sat. aq $NaHCO_3$ (200/50 mL), the phases separated, the aqueous layer extracted with EtOAc (3 × 150 mL), and the combined organic extracts were washed with sat. aq $NaHCO_3$ (100 mL) and water (100 mL). After drying ($MgSO_4$) and removal of the solvent in vacuo, the solid methyl imidate ester was dissolved in a mixture of MeOH (150 mL) and water (150 mL). After stirring for 30 min, the solution was acidified to pH 1 with 5% aq H_2SO_4 and further stirred for 2 h at rt. The cooled mixture (ice-bath) was brought to pH 9 with 2 M aq NaOH (∼125 mL), EtOAc (250 mL) was added, and the brown organic phase was separated. The aq layer was extracted with EtOAc (3 × 150 mL), and the combined organic solutions were dried over $MgSO_4$ and, after filtration, concentrated in vacuo to give a light-brown solid. Hot filtration with hexanes (50 mL) and subsequent evaporation of the solvent in vacuo afforded **2** as a beige solid (10.63 g, 49.6 mmol, 73.4%). MS (EI): *m*/*z* (%) = 214 (12) $[M]^+$, 156 (100) $[M\text{-}COOCH_3]^+$. ^{1}H NMR (500 MHz, $CDCl_3$): δ 4.02 (s, COOC H_3, 3H), 7.32 (m, 1H), 7.82 (m, 1H), 7.94 (t, J = 7.9 Hz, 1H), 8.11 (dd, J_1 = 7.7 Hz, J_2 = 1 Hz), 8.51 (d, J_1 = 7.9 Hz, 1H), 8.59 (dd, J_1 = 7.9 Hz, J_2 = 1 Hz, 1H), 8.66 (m, 1H). ^{13}C NMR ($CDCl_3$): δ 52.7, 121.6, 124.1, 124.2, 124.9, 137.0, 137.8, 147.5, 149.0, 155.1, 156.3, 165.7.

Synthesis of 3,5-Bis{6(2,2′-dipyridyl)}pyrazole (L^H). To NaH (0.83 g, 2.5 equiv) under N_2 was added a solution of **1** (2.75 g, 13.8 mmol) and **2** (2.78 g, 13.0 mmol) in dry THF (150 mL) via cannula at 0 °C, and the resulting slurry was stirred for 2 h before warming to rt and further stirring for 3 h, during which time the yellow suspension turned into a red−brown solution. Slow addition of H_2O to the ice-cooled solution to quench excess NaH (addition is continued until no noticeable gas evolution is observed) is followed by addition of a 0.5 M HCl solution (50 mL) and CH_2Cl_2 (50 mL), resulting in the formation of a white precipitate at the interface between the organic and aqueous phase. The product was obtained by filtration and subsequently dried in air. Due to the apparent insolubility in all common solvents, including DMSO, this product was applied without further characterization. The white solid (3.92 g, 10.3 mmol) was suspended in toluene (150 mL), and $H_2NNH_2{\cdot}H_2O$ (5 equiv, 3.15 mL, 65 mmol) was added via syringe. The resulting mixture was refluxed for 16 h using a Dean–Stark setup. The organic layer was concentrated in vacuo to yield $\mathbf{L^H}$ as an off-white solid (1.92 g, 5.1 mmol, 39.2% based on **2**). MS (EI): *m*/*z* (%) = 376 (100) $[M]^+$. ^{1}H NMR ($CDCl_3$): δ 7.20 (t, 2H), 7.46 (s, pz-H^4, 1H), 7.62 (d, 4H), 7.83 (d, 2H), 8.18 (t, J = 1 Hz, 2H), 8.47 (d, J = 1 Hz, 2H), 8.60 (d, 2H), 12.6 (br s, NH, 1H). ^{13}C NMR ($CDCl_3$): δ 101.8, 119.9, 121.3, 123.6, 136.7, 137.5, 148.9, 155.4, 155.8. UV−vis (8.86×10^{-5} M, MeOH): λ [nm] (ε [L mol^{-1}cm^{-1}]) 237 [32 554], 263 [30 230], 306 [23 756]. Anal. calcd (%) for $C_{23}H_{16}N_6$ (376.4 g/mol) C, 73.39; H, 4.28; N, 22.33. Found C, 73.82; H, 4.52; N, 21.61.

Preparation of $[Co_4L_4][Na(NO_3)_4](NO_3)$ (3). $\mathbf{L^H}$ (100 mg, 266 μmol) and NaO^{t}Bu (26 mg, 266 μmol) were dissolved in MeOH (50 mL) at room temperature. $Co(NO_3)_2{\cdot}6H_2O$ (77 mg, 266 μmol) in MeOH (25 mL) was then added to give a yellow solution and stirring was continued for 4 h. Filtration and removal of solvent in vacuo from the dark-yellow filtrate left a yellow solid. Slow diffusion of Et_2O into a solution of the crude product in MeOH yielded orange−red crystals of **3**·Et_2O·4MeOH (64 mg, 42%). UV−vis (3.5×10^{-4} M, MeOH): λ [nm] (ε [L mol^{-1}cm^{-1}]) 237 (139 870), 287 (112 440), 337 (sh, 77 610), 454 (sh, 5517), 519 (780), 550 (451). IR (KBr, cm^{-1}): 114 3434 (s), 3142 (w), 1601 (s), 1597 (s), 1564 (s), 1537 (m), 1483 (m), 1459 (s), 1441 (s), 1385 (s), 1312 (s), 1241 (m), 1176 (w), 1080 (w), 1054 (w), 1021 (w), 1001 (s), 825 (s), 777 (s), 699 (s), 630 (m). FAB-MS (3-NBA): *m*/*z* (%) 1737 (8) $[Co_4L_4]^+$, 1303 (8) $[Co_3L_3]^+$, 868 (40) $[Co_2L_2]^+$. HRESI-MS (MeCN): *m*/*z* (%) 930 (15) $[Co_4L_4(NO_3)]^{2+}$, 599 (45) $[Co_4L_4(NO_3)]^{3+}$, 434 (100) $[Co_4L_4]^{4+}$. Anal. calcd (%) for $[C_{92}H_{60}Co_4N_{24}]\{Na(NO_3)_4\}(NO_3){\cdot}4H_2O$ ($C_{92}H_{68}Co_4N_{29}NaO_{19}$ 2142.43 g mol^{-1}) C, 51.58; H, 3.20; N, 18.96. Found C, 51.06; H, 3.48; N, 18.42.

Preparation of $[Mn_4L_4](PF_6)_4$ (4). $\mathbf{L^H}$ (100 mg, 266 μmol) and NaO^{t}Bu (26 mg, 266 μmol) were dissolved in MeCN (40 mL) at room temperature. To this mixture was added $MnAc_2$ (46 mg, 266 μmol), followed by addition of NH_4PF_6 (44 mg, 266 μmol). Subsequently, MeOH (10 mL) was added to facilitate dissolution of the metal precursor, and a yellow solution was obtained after stirring was continued for 16 h. Filtration and removal of solvent in vacuo from the yellow filtrate left a yellow solid. Slow diffusion of Et_2O into a solution of the crude product in MeCN yielded yellow crystals of **4** (60 mg, 35%). UV−vis (1.4×10^{-4} M, MeCN): λ [nm] (ε [L mol^{-1}cm^{-1}]) 240 (150 347), 287 (110 253), 341 (83 040), 421 (778), 447 (241). IR (KBr, cm^{-1}): ν 3658 (w), 1595 (s), 1564 (s), 1533 (m), 1482 (m), 1459 (m), 1439 (s), 1310 (m), 1276 (w), 1239 (m), 1178 (w), 1161 (w), 1147 (w), 1092 (w), 1072 (w), 1054 (w), 1021 (w), 1001 (m), 835 (s), 773 (s), 696 (m), 654 (m), 628 (m). HRESI-MS (MeCN): *m*/*z* (%) 1005 (10) $[Mn_4L_4(PF_6)_2]^{2+}$, 580 (43) $[Mn_4L_4(PF_6)]^{3+}$, 43 (100) $[Mn_4L_4]^{4+}$. Anal. calcd (%) for $[C_{92}H_{60}Mn_4N_{24}](PF_6)_4$ MeCN·$2H_2O$ ($C_{94}H_{67}Mn_4N_{25}P_4F_{24}O_2$ 2378.1 g mol^{-1}) C, 47.48; H, 2.84; N, 14.72. Found C, 46.86; H, 2.74; N, 14.49.

Preparation of $[Cu_4L_4](ClO_4)_4$ (5). $\mathbf{L^H}$ (100 mg, 266 μmol) and NaO^{t}Bu (26 mg, 266 μmol) were dissolved in MeCN (50 mL) at room temperature. This mixture was added dropwise to a solution of $Cu(ClO_4)_2{\cdot}6H_2O$ (98 mg, 266 μmol) in MeCN (50 mL) to give a dark-green solution and stirring was continued for 16 h. After filtration, the solution was concentrated to ∼30 mL in vacuo and layered with hexane (15 mL) and Et_2O (50 mL). Slow diffusion yielded green crystals of **5** (60 mg, 42%). UV−vis (3.3×10^{-4} M, MeCN): λ [nm] (ε [L mol^{-1} cm^{-1}]) 229 (158 652), 273 (95 606), 311 (80 533), 361 (23 435), 647 (425). IR (KBr, cm^{-1}): ν 3432 (w), 3075 (w), 2005 (w), 1603 (s), 1567 (s), 1492 (m), 1462 (s), 1443 (s), 1431 (s), 1320 (s), 1254 (m), 1101 (s), 817 (s), 778 (s), 701 (s), 623 (s). HRESI-MS (MeCN): *m*/*z* (%) 977 (12) $[Cu_2L_2(ClO_4)]^+$, 618 (10) $[Cu_4L_4(ClO_4)]^{3+}$, 438 (100) $[Cu_4L_4]^{4+}$ and $[Cu_2L_2]^{2+}$. Anal. calcd (%) for $C_{92}H_{60}Cu_4N_{24}Cl_4O_{16}{\cdot}2H_2O$ (2189.6 g mol^{-1}) C, 50.47; H, 2.95; N, 15.35. Found C, 50.23; H, 2.85; N, 15.34.

X-ray Crystallography. X-ray data were collected on a STOE IPDS II diffractometer (graphite monochromated Mo Kα radiation, λ = 0.71073 Å) by use of ω scans at −140 °C (Table 2). The structures were solved by direct methods and refined on F^2 using all reflections with SHELX-97.[45] The nonhydrogen atoms were refined anisotropically, except those in disordered parts. Hydrogen

(45) (a) Sheldrick, G. M. *SHELXL-97, Program for Crystal Structure Refinement*; University of Göttingen: Göttingen, Germany, 1997. (b) Sheldrick, G. M. *SHELXS-97, Program for Crystal Structure Solution*; University of Göttingen: Göttingen, Germany, 1997.

Table 2. Selected Crystallographic Data for Complexes **3**–**5**

	3	**4**	**5**
formula	$C_{93}H_{64}Co_4N_{29}NaO_{16}$	$C_{103}H_{84}F_{24}Mn_4N_{28}O_3P_4$	$C_{92}H_{60}Cl_4Cu_4N_{24}O_{16}$
FW/M_r	2102.44	2561.62	2153.60
crystal size (mm)	0.50 × 0.41 × 0.32	0.49 × 0.36 × 0.25	0.50 × 0.36 × 0.24
crystal system	monoclinic	triclinic	monoclinic
space group	$P2_1/n$ (no. 14)	$P\bar{1}$ (no. 2)	$C2/c$ (no. 15)
a (Å)	20.1757(6)	14.3848(6)	25.5839(11)
b (Å)	23.7013(7)	14.5259(6)	15.2577(4)
c (Å)	20.4993(6)	27.0719(11)	22.1192(10)
α(deg)	90	92.411(3)	90
β(deg)	91.434(3)	105.214(3)	98.641(4)
γ(deg)	90	89.904(3)	90
V (A^3)	9799.5(5)	5453.4(4)	8536.3(6)
μ (mm^{-1})	0.749	0.618	1.196
Z	4	2	4
d_{calc} (g cm^{-3})	1.425	1.560	1.676
hkl range	±23, ±27, −23 − 22	±16, −17 −16, ±31	−33 − 32, ±19, ±28
θ range	1.31−24.84	1.40−24.84	1.56−27.43
reflections collected	83791	81229	62842
unique reflections (R_{int})[a]	16548 (0.0720)	18655 (0.0706)	9685 (0.0527)
obsd reflns ($I > \sigma(I)$)	13202	13464	7450
param/restraints	1287/30	1452/575	631/0
GOF	1.033	1.064	1.023
R_1 ($I > \sigma(I)$)[c]	0.0434	0.0655	0.0348
wR_2 (all data)[b]	0.1197	0.1949	0.0926
residual electron density [e Å^{-3}]	−0.712/0.758	−0.770/1.145	−0.580/0.362

[a] $R_{int} = \Sigma[|F_o^2 - F_o^2(\text{mean})|]/\Sigma[F_o^2]$. [b] $wR(F^2) = [\Sigma[w(F_o^2 - F_c^2)^2]/\Sigma[w(F_o^2)^2]]^{1/2}$. [c] $R(F) = \Sigma(F_o| - |F_c)/\Sigma|F_o|$.

atoms were placed in calculated positions and assigned to an isotropic displacement parameter of 0.08 Å^2. One nitrate anion in **3** was found to be disordered about two positions (occupancy factors 0.633(11)/0.367(11)) and was refined by using SADI (d_{N-O} and $d_{O\cdots O}$) restraints. The unit cell of **3** contains also disordered diethyl ether and methanol solvent molecules, for which no satisfactory model for the disorder was found. For further refinement, the contribution of the missing solvent molecules (1426.2 Å^3, electron count 274) was subtracted from the reflection data by the SQUEEZE[46] routine of the PLATON[47] program. In **4**, one bipyridyl sidearm was found to be disordered about two positions (occupancy factors 0.595(13)/ 0.405(13)). The length of the bond to the pyrazole ring was fixed by using a SADI restraint (d_{C-C}). Additionally, the four PF_6^- anions, and some of the acetonitrile and methanol solvent molecules, are disordered. SADI (d_{P-F}, $d_{F\cdots F}$, d_{C-N}, d_{C-C}) and DFIX restraints (d_{C-N} = 1.14 Å, $d_{C\cdots N}$ = 2.61 Å, d_{C-O} = 1.41 Å) and EADP constraints were used to model the disorder. Face-indexed absorption corrections for **5** (T_{max}/T_{min} = 0.7982/0.5620) were performed numerically with the program X-RED.[48]

Acknowledgment. We thank the Alexander von Humboldt Foundation for a postdoctoral fellowship (to J.I.v.d.V.), the DFG (SFB 602, project A16) for financial support, Benjamin Schneider for experimental assistance, and Dr. A. Claudia Stückl for EPR measurements.

Supporting Information Available: Figures S1−S6. This material is available free of charge via the Internet at http://pubs.acs.org.

IC701951A

(46) van der Sluis, P.; Spek, A. L. *Acta Crystallogr.* **1990**, *A46*, 194–201.
(47) Spek, A. L. *PLATON, A Multipurpose Crystallographic Tool*; Utrecht University: Utrecht, The Netherlands, 2007.
(48) *X-RED*; STOE & CIE GmbH: Darmstadt, Germany, 2002.